Analysis of long-term GIC measurements in transformers in Austria

D. Albert[1], P. Schachinger[1], R. L. Bailey[2], H. Renner[1], G. Achleitner[3]

[1]Graz University of Technology, Graz, Austria
[2]Conrad Observatory, Zentralanstalt für Meteorologie und Geodynamik, Vienna, Austria
[3]Austrian Power Grid AG, Vienna, Austria

Key Points:

- Measurements of GICs in power grid substation transformers have been carried out since September 2016 in Austria.
- We summarise the measurements until now and discuss data quality and sources of noise.
- An analysis , including a statistical evaluation, comparing two network models with measurement data and an attempt to a risk assessment, of the largest geomagnetic storms observed in the measurements so far is carried out.

Corresponding author: Dennis Albert, dennis.albert@tugraz.at

Abstract

Geomagnetically induced currents (GICs), a result of solar wind interaction with the Earth's magnetic field and the resistive ground, are known to flow in power transmission grids, where they can lead to transformer damage and grid operation problems. In this study we present an analysis of five years of continuous GIC measurements in transformer neutral points in Austria. Seven self-designed stand-alone measurement systems are currently installed in the Austrian 220 kV and 380 kV transmission levels, measuring currents up to 25 A. We identify recurrent geomagnetic activity in the measurements, and also find man-made sources of low frequency currents using frequency analysis. In order to support the transmission grid operators, two GIC simulation approaches are used to simulate GICs in the power grid. The first model uses measurements to derive the sensitivity of the location to northward and eastward geoelectric field components (which requires no detailed grid data), and the second model uses the detailed grid model to compute GICs from a geoelectric field. We evaluate two geomagnetic storms from September 2017 and May 2021 to discuss the effects of GICs on the power transmission grid and its assets.

Plain Language Summary

During geomagnetic storms, rapid changes in the Earth's magnetic field induce an electric field in the ground, may drive currents in the power grid. These are called geomagnetically induced currents (GICs) and they can lead to power grid operation problems and even transformer damage. In this study we present learning's from five years of GIC measurements in Austria, which have been carried out in seven different transformers in the grid. Some power grid transformers show larger susceptibility than other transformers to magnetic field variations accompanied by larger GICs. We also identify some of the sources of noise in the data such as a city subway system, and investigate two geomagnetic storms from September 2017 and May 2021 in more detail.

1 Introduction

For as long as there have been conductive networks on our planet's surface, there have been geomagnetically induced currents or GICs (Boteler & Pirjola, 1998). These currents, which are caused by variations in the Earth's magnetic field, flow through grounded conductive systems such as power grids, moving between the conductive power lines and the earth via transformers (Price, 2002). Due to the damage and disruption GICs can cause within power grid infrastructure (Molinski, 2002) such as that seen in Quebec during the March 1989 geomagnetic storm (Bolduc, 2002), modelling and measuring of potential currents is seeing increased interest due to grid operation safety concerns (Kelbert, 2020; Oughton et al., 2017).

Research into GICs in Austria began in 2014 in a study initiated by the Austrian Power Grid AG (APG) and summarised in Halbedl et al. (2014). The aim of this first attempt was to investigate possible DC currents in the Austrian high voltage power transmission network. For APG, measurements of DC are important to study the nature of the currents and possible effects on transformers, as well as the impact of DC on different equipment such as instrument transformers and protection devices. The data are also used as a planning basis for the design criteria of new transformers.

The section of the Austrian power grid under investigation in the 220 kV and 380 kV levels has 56 interconnected substations with a total length of 6,965 km of power lines and 87 transformers, spanning an area of 84,000 km^2. After the initial test measurements in 2014, more DC measurement devices were installed with the aim of a long-term measurement campaign, and the first data analysis was carried out in Halbedl et al. (2016) at the Institute of Electrical Power Systems at Graz University of Technology (IEAN,

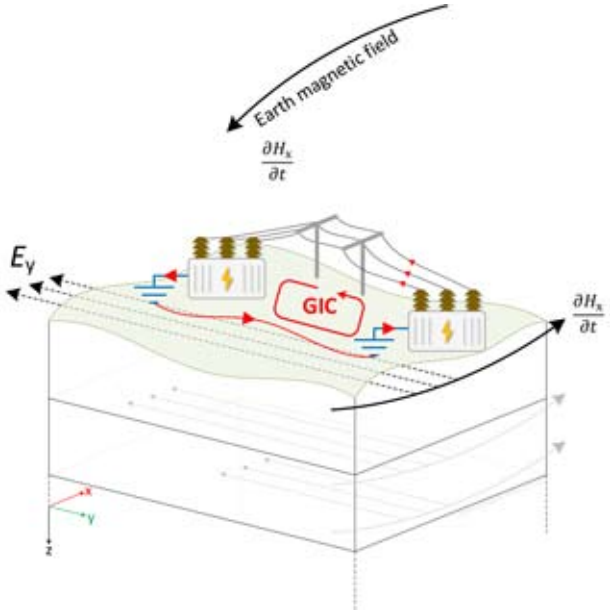

Figure 1. Depiction of geomagnetic induction and GICs in the power grid. $\partial H_x/\partial t$ are horizontal geomagnetic variations in the northward direction, and $\mathbf{E}_y$ is the corresponding geoelectric field induced in the eastward direction. The 'GIC' loop shows the loop formed between the ground and power lines, through which the GICs flow via transformers. Layers of resistive material going into the Earth show how the geoelectric field tends to lose intensity with increasing depth z.

TU Graz) and later in Bailey et al. (2017, 2018) at the Conrad Observatory for geomagnetic field measurements (ZAMG). The studies at each institute had different focus areas: the TU Graz looked in detail at the different sources of DC in the power grid and the effects on transformers, while the ZAMG focused on geomagnetic variations and the scales of possible GICs both past and future. This work continues in Albert et al. (2019, 2020).

There are now five years of measurements of DC in transformers at various locations in Austria. Worldwide, there are still few countries with GIC measurements spanning long time periods and multiple locations, with some examples being New Zealand (Rodger et al., 2017), China (Zhang et al., 2015), more recently the USA (Kellerman et al., 2021) and Finland (Pirjola, 1989).

In addition to the measurements, two GIC simulation models for the Austrian power grid have been developed based on two different geoelectric field modelling approaches.

The first model, from the IEAN, is based on the plane-wave method in combination with the power grid model. The simulation can be interfaced with a graphical user interface (GUI) and is publically available with sample data at `https://github.com/P-Schachinger/LFC_simulator` (Schachinger & Albert, 2021). The second method is also based on the plane-wave method, but operates without the detailed power grid data. Instead of the power grid data, factors for the sensitivity of each substation are derived from past transformer neutral current measurements. A third model from the ZAMG developed in the past, which is not presented here, is based on calculation of the geoelectric field on a surface with a surface conductive thin-sheet, and can be found at `https://github.com/bairaelyn/GEOMAGICA`. A comparison of different models with different de-

grees of detail was performed in Bailey et al. (2018) and summarized in Table 2 in the same publication. The results reveal only slight improvements with increasing degree of detail of the Earth model with the thin-sheet approach. Therefore, a higher degree of detail do not justify the effort for the ground modelling. However, due to the presence of the Alps, these effects could be larger in the western part of Austria, where there have been fewer measurements to date. The absence of any highly conductive coastlines makes Austria a far simpler case than e. g. the UK or Sweden.

In this paper the results of an analysis of the entire data set of DC measurements and summarise the lessons learned in the five years since the measurements started.

2 Data

2.1 DC measurement system

The IEAN transformer neutral point current (NPC) measurement system (version 3) is a self-engineered stand-alone and remote-controllable data acquisition system. The measurement system uses an active low pass filter with a cut-off frequency of 0.7 Hz to damp e. g. the 50 Hz power system frequency, meaning the sampling rate of the data acquisition can be reduced to 1 Hz. An active second order low pass filter in Sallen-Key design is preferred over a passive filter in order to reduce the filter components. This low sampling frequency allows to use a low-cost single-board computer, such as a Raspberry Pi.

The measurements of currents are done with a Hall effect closed-loop zero flux current transducer. A shunt resistor in series to the transformer neutral would change the impedance and therefore the GIC amplitude. The shunt would also be large in size because it would need to carry a high short-circuit current in the case of a line-to-ground fault. The measurement system has a guaranteed accuracy of 2 % ± 1 mA for DC in the range of ±0.1 A to ±25 A. The actual measurement accuracy for DC in the range of 1 A to 25 A is below 0.2 % ±1 mA. A technical description of the second version of the measurement system can be found in Halbedl (2019).

The measurement data is sent to an external server at the TU Graz. Before use, the data is cleaned and missing data or absolute values above 25 A are automatically flagged. The missing values are interpolated with the "Piecewise Cubic Hermite Interpolation" (PCHIP) method (Fritsch & Carlson, 1980), which results in lower amounts of overshooting in comparison to other interpolation methods. Considering the effect of interpolation in the frequency domain, the PCHIP method provides the least change in the frequency spectrum of the measured current.

2.2 GIC measurements

At the time of writing (September 2021), seven transformer neutral points in the 220 kV and 380 kV transmission levels across Austria are equipped with our GIC measurement system, as depicted in **Figure 2**. The measurement locations are named according to order of setup going from #01 to #08 (where #06 is not in use). Measurements started in September 2016 with one measurement system near Vienna in a 380 kV transformer neutral. **Figure 3** gives an overview of the runtimes of all measurement systems. Client #02 was first situated in a 380 kV neutral point in eastern Austria, before it was moved to a 220 kV transformer neutral point in central Austria. All following descriptions of #02 refer to data measured at its second location.

In much of the data up until 2021 there was a cut-off point in the measurements in the negative direction of 3.5 A (but not in the positive direction). The saturated measurement periods/days are excluded in the data statistics and further analysis. This is due the electronic design of the former transformer neutral point current measurement

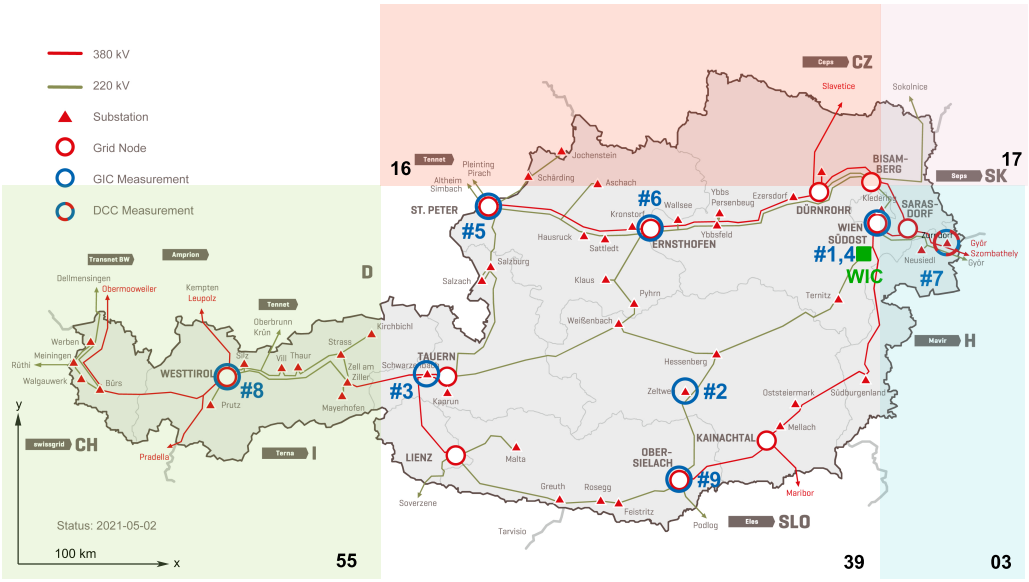

Figure 2. Substations in the Austrian transmission grid equipped with GIC measurement systems ; DCC: **D**irect **C**urrent **C**ompensation System installed and measured; colored blocks with black numbers indicate the EURHOM earth layer model.

system. The systems were installed in such a way that they were able to measure up to 25 A in one direction and up to 3.5 A in the other direction of the transformer neutral point current. With a new electronic design, established at all measurement locations from mid-2020 to mid-2021, the systems are now able to measure positive and negative currents up to an amplitude of 25 A.

The GIC events are detected with an automated algorithm. This is required because short-duration peaks, caused by switching events and faults in the power grid are also recorded. A GIC event is defined as a current with a peak prominence of at least the mean value plus the standard deviation of the analysis time span. The half width duration of the prominence needs to be at least 100 s. An automated algorithm for the detection of geomagnetic storms based on the analysis of magnetic field variations was presented in Bailey and Leonhardt (2016).

2.3 Geomagnetic field data

All measurements of the local geomagnetic field in Austria refer to those carried out at the Conrad Observatory, a subterranean tunnel system located near Muggendorf in Lower Austria. The observatory is an INTERMAGNET-quality (1 sample/sec) geomagnetic observatory (see `https://intermagnet.org/` for more details) with measurements starting in 2014. Only the x- and y-components of the field (corresponding to the northward and eastward geomagnetic field directions, respectively) are used in the analysis. Vertical (z) field variations, which generally do not contribute to geomagnetically induced currents at the surface, are ignored (Boteler & Pirjola, 2017). The individual horizontal components are also combined into the horizontal magnetic field strength component B that describes only the intensity in the 2D surface plane (where $B = \sqrt{B_x^2 + B_y^2}$). The geomagnetic variations $\mathrm{d}\boldsymbol{B}/\mathrm{d}t$ are expressed in change in field strength per timestep, i. e. nT/min.

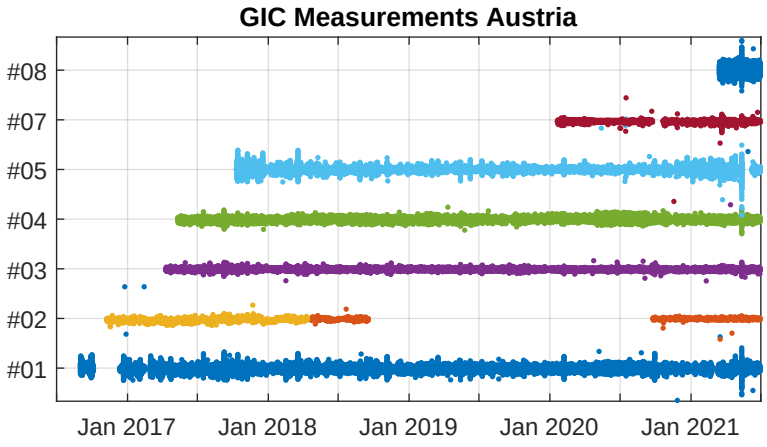

Figure 3. Measured current in A over the run times of installed measurement systems from #01 to #08. (The #06 is not in use.) The measurement device #02 moved location in 2018, hence the two different colours.

2.4 GIC Simulation

The geomagnetic storms that drive GICs lead to changes in the Earth magnetic field ($\mathrm{d}\boldsymbol{B}/\mathrm{d}t$) ranging from tens of nano Tesla (nT) up to several thousand of nT per minute depending on the geomagnetic storm and the geographical location. As depicted in **Figure 1**, the magnetic field propagates into the electrically resistive subsurface, where it induces an electric field that can be described by Faraday's Law of Induction. Under the assumption that the field propagation can be treated as a plane-wave going into the Earth (Boteler & Pirjola, 2017), solving the differential Maxwell equation with the Euler approach results in the following equations for the electric field in the northward direction (E_x) and in the eastward direction (E_y):

$$\mathrm{j}\omega\mu\frac{\partial H_\mathrm{x}}{\partial z} = -\frac{\partial^2 E_y}{\partial z^2} = -\mathrm{j}\omega\mu k E_\mathrm{y} \rightarrow -E_\mathrm{y} = -E_0 e^{kz(1-\mathrm{j})} \tag{1}$$

$$-\mathrm{j}\omega\mu\frac{\partial H_\mathrm{y}}{\partial z} = \frac{\partial^2 E_\mathrm{x}}{\partial z^2} = \mathrm{j}\omega\mu k E_\mathrm{x} \rightarrow E_\mathrm{x} = E_0 e^{kz(1-\mathrm{j})} \tag{2}$$

where $k = \sqrt{(\omega\mu\sigma)/2}$. The variables ω, μ, σ, H, E j, and z are the angular frequency, the Earth permeability, the electric conductivity, the magnetic field, the electric field, the imaginary unit, and the downward direction into the Earth, respectively. **Equations 1** and **2** imply that the electric field decreases with increasing penetration depth z. Therefore, integrating the electric field along a closed loop, e. g in the y- and z-direction (**Figure 1**) results in an electromotive force (emf) unequal to zero. This emf drives GICs in the loop formed by the power grid connected to ground and the ground itself. The work done by emf on the electric charge can be measured as a virtual electric potential around the loop. Further information on the electromagnetic field calculations can be found in Simonyi (1971) and in Simpson (2005).

Two different approaches for GIC calculations are compared to measurements: the first uses the LFC (low frequency current) simulator tool from Schachinger and Albert (2021), and the second approach is computed with a fit of the geoelectric field components ($\mathrm{E_x}$ and $\mathrm{E_y}$) to the GIC measurements (**Equation 3**).

The LFC simulator uses the plane-wave method from Pirjola (1982) to calculate an electric field in the Earth's surface. The plane-wave method is sufficient approximation for mid-latitude countries such as Austria, because the magnetic field variations are dominated by the horizontal field component. The field-aligned current system resulting in vertical field components has a lower influence, due to large geographically distance. The resistive Earth itself is model with 1D layers from the European Rho Model (EURHOM, Ádám et al., 2012). Most of Austria can be described by two different resistivity models, one for the alps in the west (EURHOM #55) and one for the flat lands in the east (EURHOM #39, Bailey et al., 2018). A Comparison of the different models, including the EURHOM models can be found in Bailey et al. (2018). In contrast to the Lehtinen-Pirjola method (Lehtinen & Pirjola, 1985), we use the nodal admittance matrix method, which is more common to use in the field of electrical engineering (Halbedl, 2019). However, the two methods are considered mathematically equivalent (Boteler et al., 2014). The power grid is modeled as a DC network with voltage sources between the substation grounding and the resistive earth. The potential of all other earth reference points are changed relative to one overall reference point. This is only valid for uniform electric fields over a certain area, however, it simplifies GIC calculation without losing much quality of the calculated GICs (Halbedl, 2019; Boteler & Pirjola, 1998).

The second GIC modelling approach is based on the method described in Pulkkinen et al. (2007) and applied for example in Torta et al. (2012). The geoelectric field is calculated using the plane-wave method using EURHOM model #39, because, regardless of where the GIC measurements were made, the geoelectric field modelled using #39 results in GICs that match the measurements well and better than any of the other models used, implying this is a good approximation for most of the region. We expect that small-scale deviations do exist, although we have yet to find any such locations. The GICs at different substations are calculated from the geoelectric field components by applying a fit to the following equation:

$$GIC_{\mathrm{j}} = a_{\mathrm{j}} \cdot E_{\mathrm{x}} + b_{\mathrm{j}} \cdot E_{\mathrm{y}} \tag{3}$$

where j is a specific substation measurement point in the power grid, and a_{j} and b_{j} are substation-specific coefficients that describe the contribution from each geoelectric field component and have the units A·km/V. The substation coefficients need to be recalculated if the configuration of the power grid changes. The fit (**Equation 3**) is applied to recent DC measurements - specifically a period in May 2021 with larger measured DC that undoubtedly has geomagnetic sources to reduce input from other sources - and a_{j} and b_{j} can be determined using the equations in Pulkkinen et al. (2007) or by carrying out a least-squares fit. Applying the method described in Pulkkinen et al. (2007), the substation coefficients a_{j} and b_{j} incorporate uncertainties from the electric field calculations, e. g. due to the limited Earth layer modelling.

3 Analysis

An analysis is carried out of the entire DC measurement data set by first providing an overview of each measurement station statistically and then by evaluating the different sources of DC both geomagnetic and man-made source are identified.

3.1 Overview of data

Table 1 lists the transformer neutral point current data statistics. For the calculation of the statistics, outages and measurement errors are removed. Switching events, which can exceed the measurement limit of $\pm\,25$ A, are not removed. The maximum current refers to GIC events and not to switching events. These events are checked both manually and with a peak detection algorithm.

Table 1. Summary of the data properties (1-sec data) at each client. μ is the mean, σ the standard variation, and DC_{max} the maximum current measured to date caused by a geomagnetic event (i. e. not a data spike or transformer switching events). The column "Sensitivity to E_x/E_y" provides the contribution of each geoelectric field component (in percentage) to the measured GICs according to the GIC fit of modelled E to recent DC measurements. In brackets, r denotes the Pearson's correlation coefficient between the GIC fit and measurements (clean days).

Client #	n_{days} raw	n_{days} clean	μ A	σ A	DC_{max} A	Date of DC_{max} UTC	Sensitivity to Ex/Ey % from E_x / % from E_y
01	1671	1651	+0.13	0.33	-8.41	2021-05-12 12:21	49/51 ($r = 0.86$)
02	479	427	-0.12	0.02	+0.83	2021-05-12 12:20	44/56 ($r = 0.84$)
03	1583	1522	-0.20	0.03	-2.42	2017-09-08 23:02	45/55 ($r = 0.72$)
04	1564	1512	+0.06	0.23	-4.57	2021-05-12 12:20	36/64 ($r = 0.85$)
05	1383	1330	-0.07	0.21	-13.83	2021-05-12 12:20	06/94 ($r = 0.89$)
07	579	492	-0.48	0.14	-2.72	2020-09-04 14:18	50/50 ($r = 0.85$)
08	159	105	+0.24	0.76	+9.31	2021-05-12 12:48	76/24 ($r = 0.57$)

We see that the stations experience very different levels of DC, with some having experienced GICs around 10 A and greater (DC_{max} in #01, #05 and #08) and others not even exceeding a maximum of 1 A such as #02 during a geomagnetic storm. Almost all of the peak GICs occurred during the May 2021 storm (which will be looked at in more detail later in this work). There are also very different levels of noise (σ) ranging from extremely quiet in #02 and #03, and very high levels in #01 and #08.

One question we can ask is how much of the measurements can be explained by geomagnetic sources? Included in the last column is an estimate of the contribution of each geoelectric field component to the GICs measured at each location. This was computed from a fit of the GIC measurements (interpolated to a sampling rate of one minute) to the geoelectric field components modelled from geomagnetic field variations according to **Equation 3**. The values are for data from the week of 2021 May 9^{th} - 16^{th}, which included a geomagnetic storm and some of the largest DC measurements to date. The r value in brackets gives the Pearson's correlation coefficient achieved by the fit. (For the stormy section alone on 2021 May 12^{th}, r ranges from 0.90 to 0.97 at all stations except for #07 and #08, where it is 0.85 and 0.82, respectively). As the correlation is generally very high, we can deduce that the signals seen in the stations can be explained by the geoelectric field variations for the most part. Some are modelled better from E than others, often those with greater levels of measured DC (e. g. #01 and #05). The lower r values for #08 are likely due to the very large noise level measured at that particular substation. In general, the SNR and the GIC amplitude is related to the power grid topology (line orientation and center/end node/substation). In addition to geomagnetic field variations, other transformer neutral point current sources should be considered, in order to judge the actual GICs in the context of a risk analysis for the power grid and its assets.

In the last column in **Table 1**, most stations are somewhat balanced in contribution from both field directions, but #05 stands out by having roughly 94 % of the currents induced by the eastward geoelectric field component alone. Client #05 is located at a transformer at the end of a long east-to-west 380 kV transmission line and therefore highly sensitive to eastward electric fields (E_y), which result from changes in the geomagnetic field in the x-direction (dB_x/dt), mainly caused by the ring current, due to the location of Austria in the mid-latitude region.

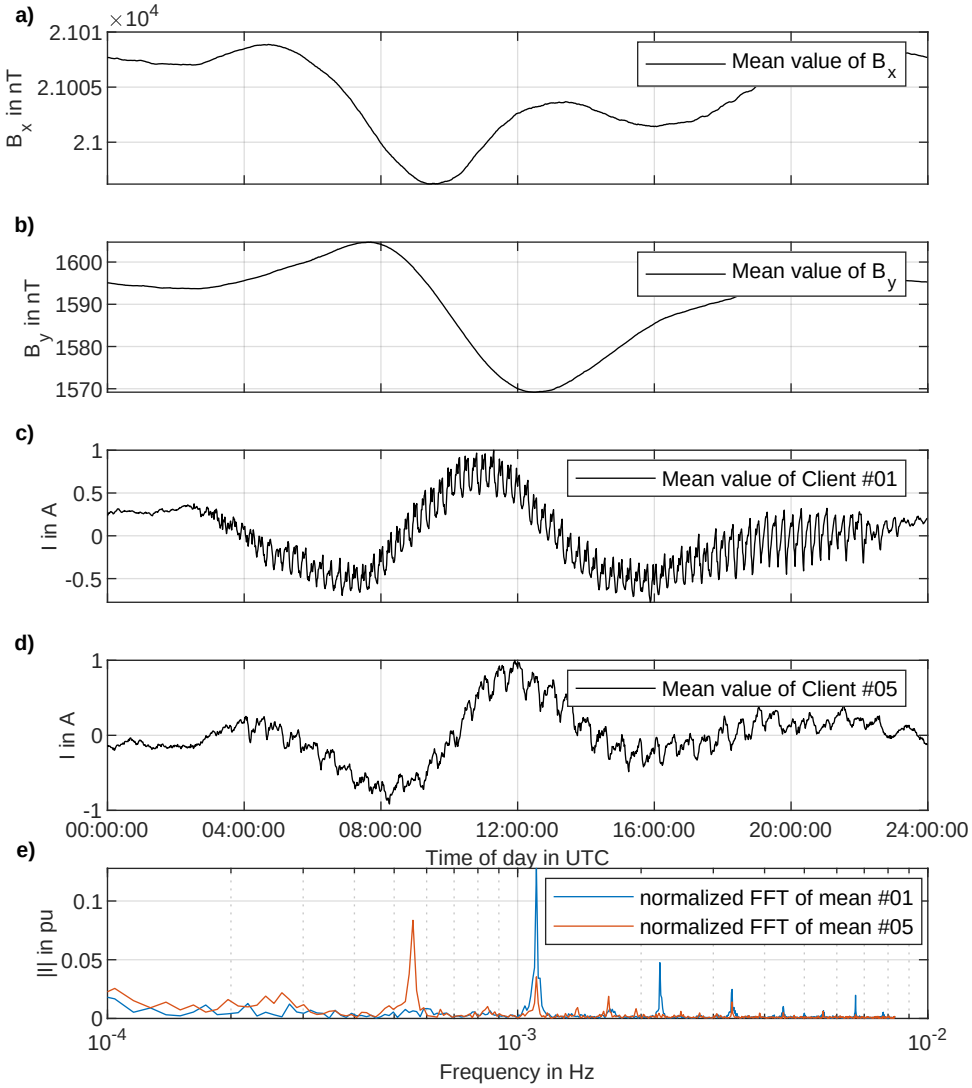

Figure 4. Mean minute values of geomagnetic field measurements a) B_x and b) B_y, and DC measurement clients c) #01 and d) #05; e) shows an excerpt from the normalized FFT of the mean from #01 and #05

Among the many signals seen in the DC measurements, there is a typical daily pattern, similar to the geomagnetic field solar quiet variation. This quiet time variability in transformer DC measurements has recently been investigated in detail in Kellerman et al. (2021). **Figure 4a)** and **d)** shows the calculated mean values for each minute of a day for magnetic field measurements and GIC measurement clients #01 and #05. For clients #01 and #05, 1,650 days and 1,330 days, respectively, were superimposed and the mean value of every minute was calculated. The magnetic field measurements have fewer data gaps, therefore about 1,740 days were used for the mean value calculation. This reveals that there are recurring neutral point currents with different time periods at different measurement points that are not caused by variations in the Earth's mag-

netic field. The excerpt of the fast Fourier transform (FFT) analysis of the mean values of #01 and #05 in **Figure 4e)** shows the dominant frequency shares, produced by other sources than geomagnetic field variations. For #01 these are sources with periods of 15 minutes and faster. These shares are also present in the frequency spectrum of #05, however, the main fast components have duration times of 30 minutes. For comparison purposes, #01 and #05 were normalized to their peak value before performing the FFT.

The alleged time shift between the two curves in **Figure 4c)** and **d)** likely has two main causes: first, the measurement systems are set to UTC time, although there is a difference in local time between the two clients of about 9 minutes as they are 250 km apart. Second, the sensitivities to changes in the different components of the geomagnetic field (resulting E-fields E_x and E_y have their maxima at different times) of the transformers in the two substations is quite different, as one is more sensitive to variations in the x-direction than the other. Another interesting effect that can be seen in **Figure 4c)** and **d)** is the small offset in both measurement clients. Although the measurement systems were calibrated during installation, the overall mean value is not zero. This is likely caused by constant DC currents unrelated to geomagnetic variations. For low frequencies the measurements from client #05 fit the B_x field qualitatively very well.

3.2 Noise sources

As can be seen from **Table 1**, there are varying levels of noise in the different measurements (mean μ and standard deviation σ). Some of this can be explained by location. Client #01 is located at the edge of the city of Vienna, where it is more likely that the noise is caused by by earth-leakage currents from technical/man-made systems. Client #05 is located approximately 115 km east of the city Munich and approximately 50 km east of a north-south railway transit corridor. The increased noise could be caused by earth-leakage currents from the city of Munich, where there is also a DC powered subway system operating, and by stray currents from the railway transit corridor/system.

Apart from these general noise sources, other sources of DC have been found in the measurements over the years. So far we have been able to identify the Vienna DC powered subway system as one contributor to the transformer neutral point currents. Another source of DC transformer neutral point currents are cathodic corrosion protection systems of power plants and pipelines (Beltle et al., 2017). In addition, the galvanic coupling of the cathodic protection system and the transmission grid, hybrid AC/DC transmission lines are coupled through DC ion currents (Pfeiffer et al., 2015). We are also currently investigating the effects of power electronics, such as the converters from renewable energy resources (e. g. wind and photovoltaic, (Gertmar et al., 2005)), and the effects of trading at the electrical energy market. Solar radiation can be excluded as a source (Albert et al., 2020).

3.2.1 Vienna DC subway system

As first described in Halbedl (2019), leakage currents of public transportation systems are measured in several measurement systems in Austria. This was identified by analysing the frequency spectrum of the currents, as well as by comparing the operating hours of the Vienna subway with patterns in the neutral point currents. During the nights from Sunday to Thursday, the subway operation stops for a few hours (from roughly 00:30 am till 05:00 am), and on the nights of Friday and Saturday, the subway stays in operation through the night. The operating times can be seen clearly in **Figure 5a)**, which shows the root-mean-square in the DC measurements over 8-day periods. The currents clearly stay at a higher level during weekend nights rather than dropping to around 0 A, as they do on weekdays. As can be seen in the plot, these stray currents contribute roughly 0.2 A to the measurements during the day.

Due to the COVID-19 restrictions in public transportation, the Vienna subway stopped its weekend nightly operations and also reduced the number of trains in operation. This change in operating hours can be seen in **Figure 5b)**, in which there are also lower neutral point currents during the weekend nights. Lowes (2009) also identified unintended earth-leakage currents from DC railways systems, which caused interference during geophysical surveys.

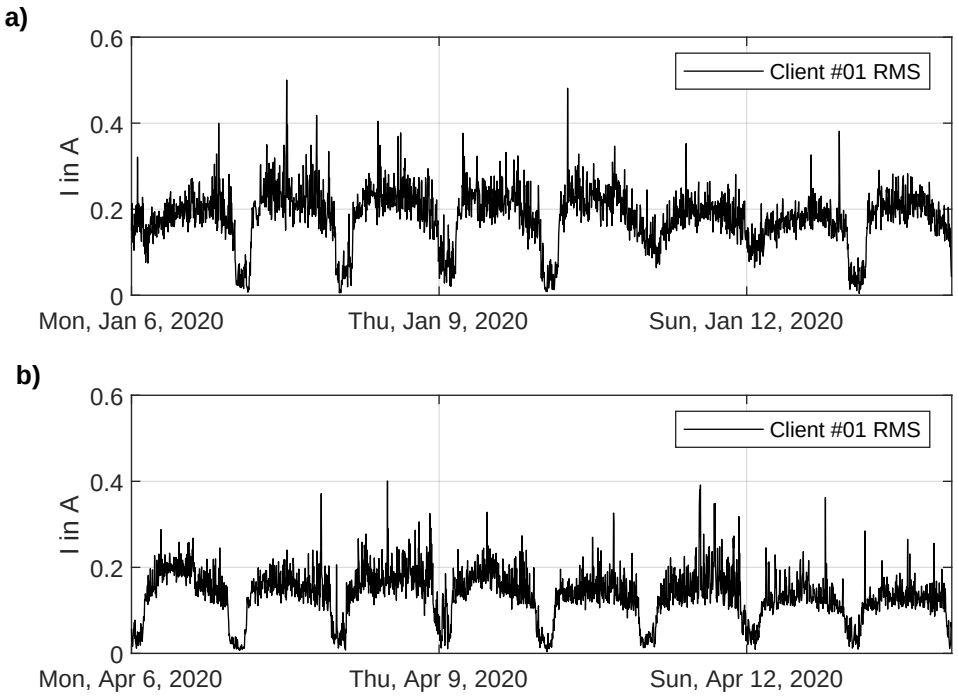

Figure 5. Influence of Vienna DC subway leakage currents on transformer neutral point currents as seen in: a) normal operation, including over weekend nights, where the subways stays in operation, and b) during COVID-19 lockdown restrictions, when the subway stopped extended operation during weekends nights.

3.3 Recurrent geomagnetic activity

Having identified some sources of noise in the data, we now look more closely at the geomagnetic signals present in the measurements, among which are recurrent geomagnetic activity. Geomagnetic activity has long been known to recur roughly every 27 days (Richardson et al., 2000; Tsurutani et al., 2006) due to the persistence of high speed streams and corotating interactions regions (Alves et al., 2006) over more than one solar rotation or Carrington rotation. This is evidenced by recurrent mild geomagnetic storms. A recent study by Gil et al. (2021) has shown that this is also observable in power grid observations.

Figure 6 shows the DC measurements across each Carrington rotation (roughly 27 days long). To produce this plot, each Carrington rotation was split into 100 time windows (each window one pixel), and the maximum absolute DC or $\mathrm{d}H/\mathrm{d}t$ (variation in the horizontal magnetic field strength) was found for each window, while the solar wind speed, which clearly show corotating interaction regions in the solar wind, is plotted be-

neath. The recurrent geomagnetic activity can be seen in both upper plots, although in the DC measurements it is not as pronounced as in geomagnetic variations partly because there is a constant level of noise in the DC measurements, which some of the geomagnetically induced currents can get lost in. Plot (d) shows the cross-correlations between each time series at different time shifts. The highest correlations are between $\mathrm{d}H/\mathrm{d}t$ and the solar wind, likely because there is a better signal to noise ratio. The 27-day recurrence from solar wind structures is clearly visible in the secondary peaks at time shifts of 27 and 54 days. The coherence between daily variations in $\mathrm{d}H/\mathrm{d}t$ and measured GICs are also visible.

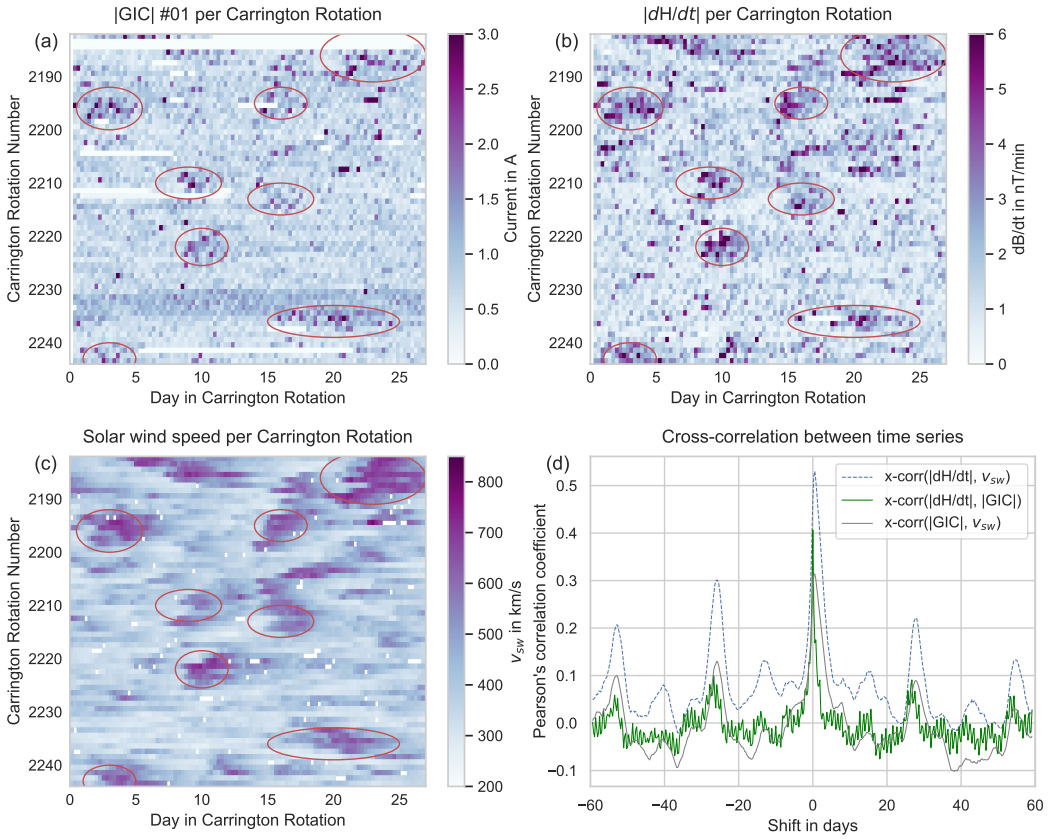

Figure 6. Influence of recurrent geomagnetic activity from high speed streams and corotating interaction regions. (a) Measurements of GICs at station #01 (from which we have the longest time series), (b) horizontal magnetic field variations (from the Conrad Observatory in Lower Austria), (c) the measured solar wind speed showing corotating interaction regions, and (d) the cross-correlation between the time series for different shifts in time. Each variable is plotted for each 27-day Carrington Rotation (x-axis) across all Carrington rotations from September 2016 till May 2021 (y-axis, time increasing from top to bottom). Examples of recurring activity visible in both GIC and magnetic data that last longer than one rotation are marked with red circles in both plots. White spaces in both plots are data gaps. The recurrent activity can be seen in the secondary cross correlation peaks at time shifts of 27 and 54 days.

3.4 Events during the observation period

Throughout the duration of the measurements and the progress of solar cycle 24 into cycle 25, we have observed some minor and moderate geomagnetic storms. Here we present the measurements and a brief analysis of two storms. For each storm, we also consider the cumulative GICs that would have been seen during that period by calculating an additional parameter, $\mathrm{GIC_{sum}}$.

3.4.1 Calculation of GIC-Sum

In the Austrian power grid, transformers in the 220 kV and 380 kV levels are generally solidly grounded, without any resistance between the transformer neutral point and the substation grounding. GICs can enter and exit the transmission grid via the transformer neutral points. The transformers are designed to handle alternating magnetic flux in the magnetic transformer core, and direct magnetic flux can cause saturation of this magnetic core material. Operating with a saturated transformer core has short-term and long-term effects on the transformer. Short-term effects (scales of minutes) are half-cycle saturation leading to current and voltage distortion, which are the reasons for the increased non-active power demand of the transformer. The increased non-active power demand can cause undesired voltage drops and power system instabilities. If saturation in the transformer core lasts over multiple hours or even days, the voltage and current distortion also causes transformer heating, which can be considered as a long-term (hours) effect. Short- and long-term effects of GICs on transformer are also discussed in Gaunt et al. (2020). The transformer heating is due to the increased current and stray flux in the metallic tank and transformer reinforcements. GICs with comparable short duration and high amplitudes as well as GICs with comparable low amplitude and long duration can cause the transformer hot spot temperature to increase above the acceptable design limits. A further increase in temperature causes a loss of insulation and internal transformer failures.

In order to quantify and consider the afore-mentioned long-term effects, the $\mathrm{GIC_{sum}}$ value is calculated according to **Equation 4**. The $\mathrm{GIC_{sum}}$ value is the accumulated absolute current amplitude over a fixed time period with a fixed sample rate, which in this case is a time period of one hour and a sampling rate of one second. The data presented in **Figure 8** and **Figure 9** are a first attempt to quantify and take into accumulated GIC load on transformer. For a further risk analysis, a guidance containing a threshold level where GICs starts to contribute to an accumulated exposure and different alert levels should be provided. This guidance would be need to be adapted for different transformer designs.

$$GIC_{\mathrm{sum}} = \int_{t_1}^{t_2} |\mathrm{GIC}(t)| \, \mathrm{d}t \tag{4}$$

3.4.2 May 12 2021 Event

On 2021 May 9$^{\mathrm{th}}$, a CME associated with a filament eruption was detected. This reached the Earth and became geomagnetically effective on 2021 May 12$^{\mathrm{th}}$. During this event, a maximum Kp value of 7 (Geoforschungszentrum Potsdam, 2020) was reached between 12:00 and 15:00 UTC. At 14:00 UTC the Dst value reached the minimum of -61 nT (World Data Center for Geomagnetism, Kyoto, Japan, 2021). The maximum amplitudes of currents measured in the Austrian transmission grid were 13.83 A and 9.31 A in clients #05 and client #08, respectively. **Figure 7** shows the measured currents of three transformers and the corresponding results of the LFC simulator tool and a fit of the geoelectric field to the data (GIC fit). For the clients #01 and #05 in **a)** and **b)**, the simulated currents fit the measured currents very well (Pearsons correlation coefficient r equals 0.84 and 0.96, respectively), however the results from the LFC simulator

for client #08 in **c)** do not match well $r = 0.22$ despite the fit matching the current well $r = 0.81$. This is probably caused by inaccurate grid data or uncertainties in the Earth layer model.

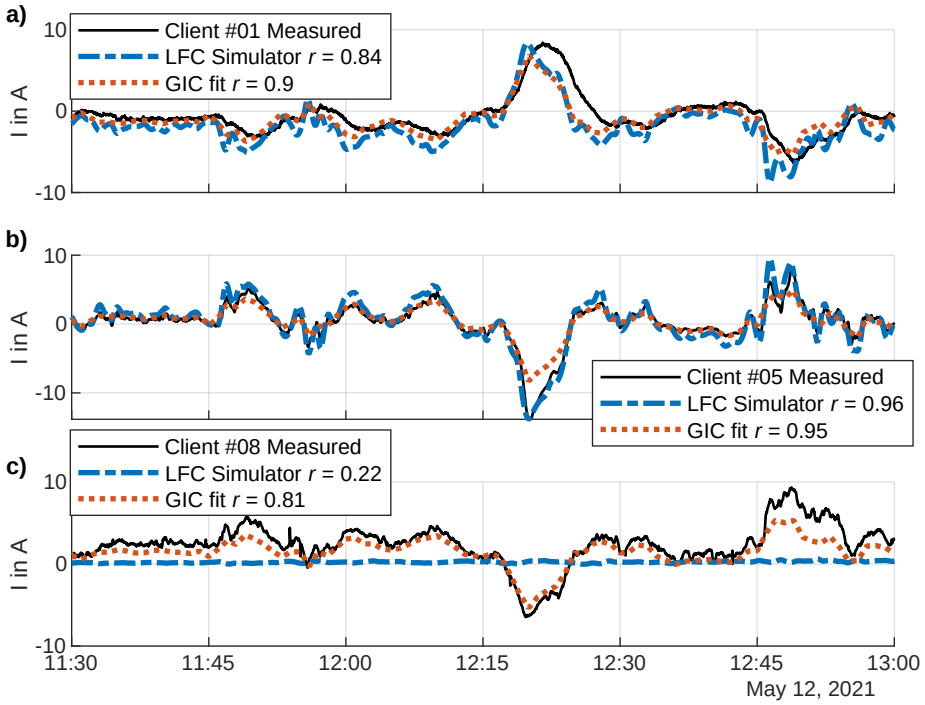

Figure 7. Measured currents during the May 2021 event, related simulation results of two calculation approaches and corresponding Pearson correlation coefficients r on May 12, 2021. The selected transformers show the highest currents: a) client #01, b) client #05 and c) client #08 (the deviation of the results from the LFC simulator are probably due to inaccurate grid data of this region).

In **Figure 8a)**, **c)** and **e)** the 1 h GIC_{sum} value for the disturbed day May 12th is plotted, in **b)**, **d)** and **f)** the 1 h GIC_{sum} value for a comparable quiet period is plotted alongside. During the quiet period, the maximum Kp value was 1-. Although the highest current amplitude was measured at client #05 (13.83 A), the highest GIC_{sum} value was reached at client #08. Clients #01 and #05 show a similar GIC_{sum} pattern during both the geomagnetic disturbance and the quiet period. Both transformers were exposed to comparable GIC_{sum} currents during a 1 h period.

Similar to the correlations done by Choi et al. (2015), **Figure 9** shows the correlation between changes in the magnetic field and resulting GICs. As magnetic field measurements in nT/min are calculated for the x- and y-directions. The related changes in measured currents at three measurement systems are given in A/min. This reveals the sensitivity directions of these stations: client #01 shows in **a)** and **b)** high correlations between changes in neutral point current and changes of the geomagnetic field. **c)** and **d)** show a higher sensitivity of client #05 to changes in x-direction, which matches with calculations in Halbedl (2019). The currents at client #08 are in general higher than at #05, however, the changes caused by geomagnetic variations during this event were smaller and a clustering can be seen in **f)**, which also indicates a lower sensitivity on changes

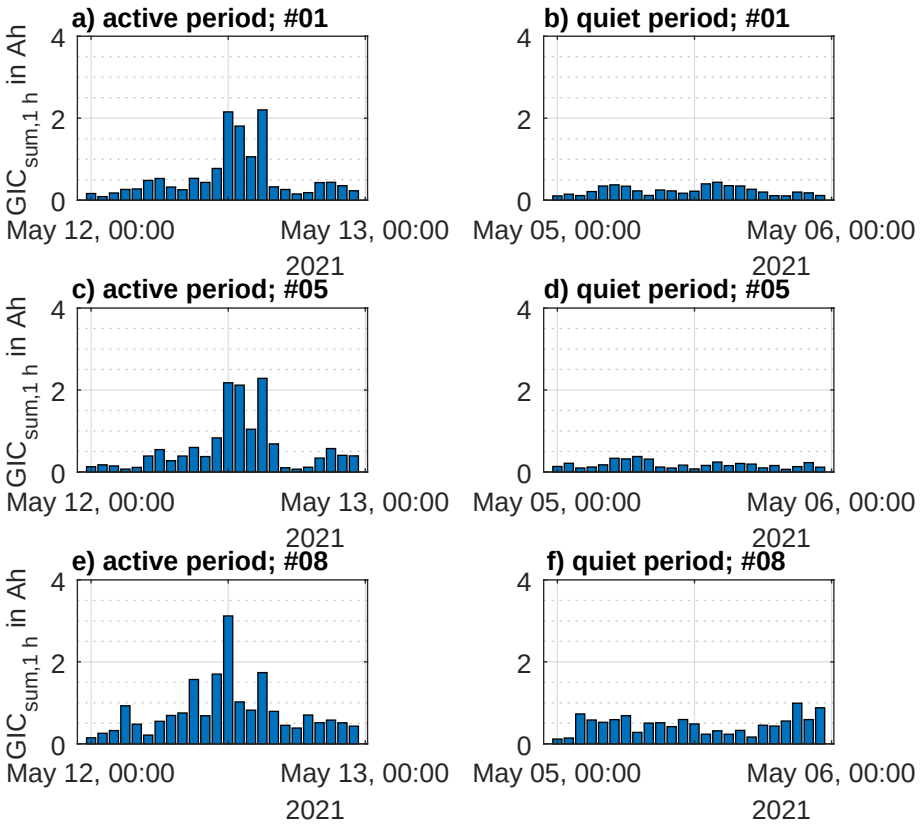

Figure 8. Cumulative 1 h GIC_{sum} of client #01 for May 2021 storm (a, c, e) and quiet (b, d, e) period during May 2021

in y-direction. The visual determined sensitivities to geomagnetic fields in **Figure 9** also match with the sensitivities to geoelectric fields in **Table 1**.

3.4.3 September 8-9 2017 Event

The September 2017 event was associated with a X9.3 flare from solar active region (AR) 12673, which is regarded as the largest in solar cycle 24. A maximum Kp value of 8+ (Geoforschungszentrum Potsdam, 2020) was reached between 12:00 and 15:00 UTC, although the maximum current amplitude only reached 5.11 A at client #01. During the September 2017 event, three measurement systems (#01, #03, #04) were active. The current amplitude at client #03 is less than half the amplitude at client #01, therefore only GIC_{sum} value of client #01 and #04 are plotted in **Figure 10**. This is a particularly interesting comparison because the two are located in the same substation in the 220 kV and 380 kV voltage levels.

Again, the measured currents are compared with the two calculation approaches of LFC Simulator and GIC fit. Unfortunately, the September event was measured with the first version of the measurement system, therefore some of the peak values are cut off because of the -3.5 A limit in the measurement device, and saturated GIC measurements imply that the actual GICs were larger. As the Dst value during the September

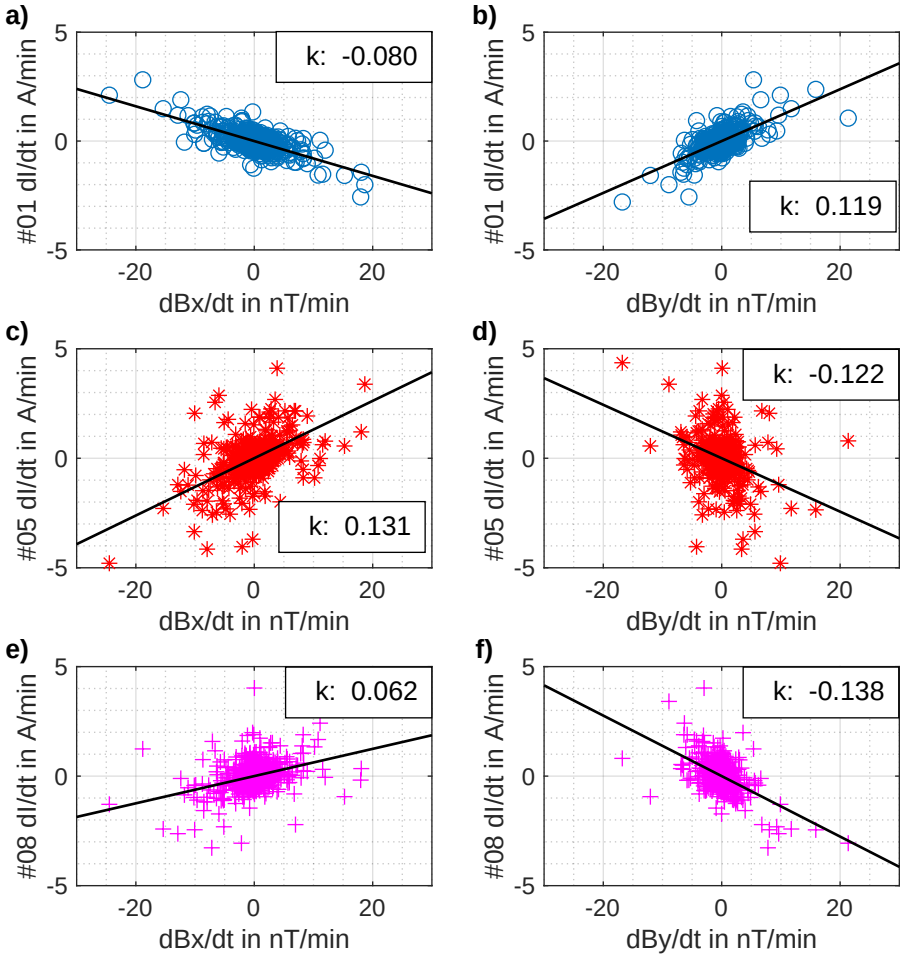

Figure 9. Correlation of $\mathrm{d}B/\mathrm{d}t$ and the resulting change in neutral point currents $\mathrm{d}I/\mathrm{d}t$ during the 2021 May 12$^{\mathrm{th}}$ event: a-b) client #01, $\mathrm{d}I/\mathrm{d}t$ standard deviation $\sigma = 0.297\,\mathrm{A/min}$, c-d): client #05 $\sigma = 0.645\,\mathrm{A/min}$, e-f): client #08 $\sigma = 0.461\,\mathrm{A/min}$. The slope k of the black least-squares fit line is also shown.

2017 event (-122 nT) was exactly twice the Dst value during the May 2021 event (-61 nT), the GIC during the September 2017 event is expected to be in the range of 25 A.

In **Figure 11a)** and **c)**, the 1 h $\mathrm{GIC_{sum}}$ value for the most disturbed period in September 2017 is plotted, and in **b)** and **d)** the 1 h $\mathrm{GIC_{sum}}$ value for a comparable quiet period is plotted. During the quiet period the maximum Kp value was 2+. Note that client #01 is a 380 kV transformer neutral measurement and #04 a 220 kV measurement in the same power grid substation. Due to the increased circuit resistance in the 220 kV level, the transformer neutral currents are usually lower than those in the 380 kV transformer neutral, and we see they are roughly half as large in #04 as they are in #01. The highest current amplitude during the September 2017 event was measured at client #01 (5.11 A), the highest $\mathrm{GIC_{sum}}$ value was also reached at client #01 (1.9 Ah). The transformer at client #04 in the same substation as client #01 was exposed to a 1.1 Ah during the same

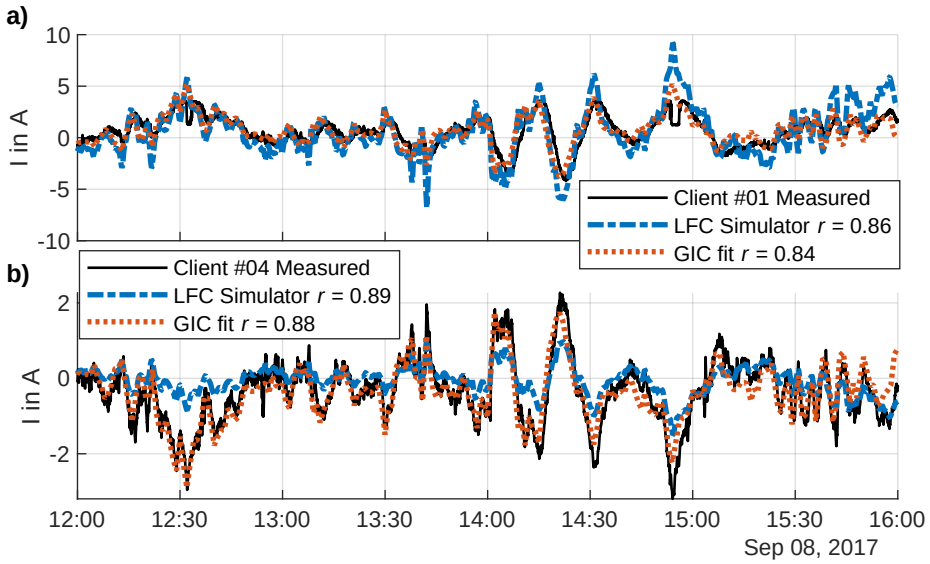

Figure 10. Measured currents during the September storm 2017 and related simulation results of two calculation approaches. The selected transformers show the currents at two different neutral points in the same substationand the corresponding Pearson's correlation coefficients: a) client #01, b) client #04; the drop in the measurement of client #01 after 12:30 UTC and before 15:00 UTC is caused by maximum current measurable with the first version of the measurement system.

time period. During the quiet period with no geomagnetic activity (Kp 0o), the transformer at client #01 and #04 were exposed to max. 0.33 Ah.

4 Discussion

The measurements covered a period of particularly low levels of geomagnetic activity throughout the end of solar cycle 24 and the beginning of cycle 25. The maximum Kp of 8- was reached during the September 2017 storm. During the last years of measurement, the geomagnetic activity was comparably low with very few periods of increased activity. Nevertheless, with the recent storms we now have sufficient data to reliably calculate the GICs in the Austrian power grid, which is unfortunately low for studying larger GIC events, however due to the relaxation of maximum measurement limits in the past year, we now have sufficient data to estimate GIC levels from recent storms.

By splitting the GIC measurement data into time intervals matching Carrington rotation intervals, recurring solar events could be identified in **Figure 6**. High recurring changes in the magnetic field with time periods of 27 days can be seen magnetic field measurements as well as in neutral point measurements in the power grid. This underlines the sensitivity of the power transmission grid, also to comparable small changes in the Earth magnetic field. Small changes in the Earth's magnetic field can also have negative effects on the power grid. Low level GICs cause an increased power loss in the system due to increased transformer windings losses and losses on the overhead transmission lines (Forbes & St. Cyr, 2010).In Addition, the allowable transformer load can be reduced by GICs (Girgis & Ko, 1992).

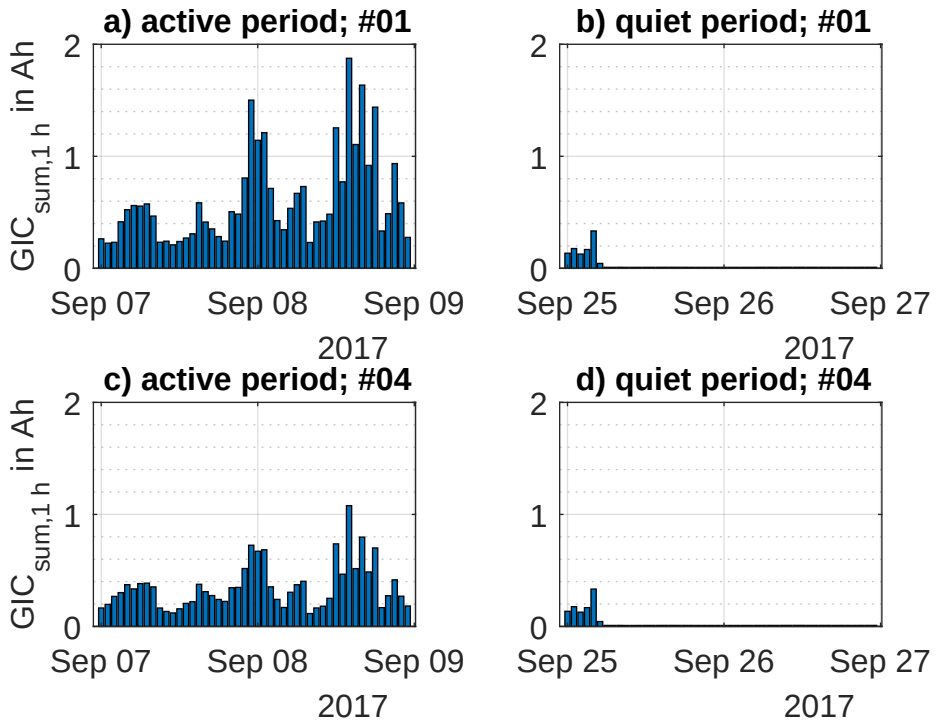

Figure 11. Cumulative 1 h GIC_{sum} for September 2017 storm (a, c) and quiet (b, d) period (data in during the quiet periods are below 0.02 Ah) during September 2017

Calculating mean values per minute for measurement periods reveals different noise sources with different frequencies in the power grid. The noise sources do not only have specific frequency spectra, they also show daily patterns, with changes every 15 or 30 minutes. One of the noise sources was identified: by comparing time patterns of GIC measurements, the influence of public transportation on transformer neutral point currents was discovered. A change in the subways timetable due to COVID-19 restrictions, confirmed this theory. Typically, the Vienna subways stops operation during weekday-night and continuous operation in weekend nights. However, this changed in March 2020 due to COVID-19 restrictions. This effect on GIC measurements could only be derived because of continuous and geographical distributed measurements. Further man-made sources of low frequency currents in the transformer neutral point are currently investigated at the time of writing, but require measurements with sample rates well above 1 Hz. To address this, temporary measurement recorders are being installed in various measurement locations.

The measurements are used for analyzing the influence of GICs on transformers and calculating the theoretical influence on the power grid. However, there are additional continuous long term measurements in power grids available. Phasor measurements units (PMU) provide data from voltage, currents, angle and frequency measurements in the power grid. The correlation of PMU data with high GICs will be done in future studies. Combining data of multiple measurement types during geomagnetic active periods could also reveal more direct influence on power grids, e. g. changes in power flow or reactive power consumption. The combination could also reveal more noise sources in the power grid DC measurements.

In addition to the current measurements, the GIC_{sum} value was calculated to evaluate long-term effects of GICs on power transformers in addition to short-term effects. The materials used in the transformers are designed for a specific lifetime, and any increase of temperature above the design limits reduces the transformer lifetime (loss-of-life). Therefore, a thermal assessment of the different transformer types in the fleet should be carried out in order to determine the loss-of-life of transformers exposed to GICs. Regarding transformer overheating, Raith (2019) indicates that, for a specific transformer design, a GIC_{sum} value of 1,000 Ah, would be permissible without any overheating of the transformer. Note that the 1,000 Ah could be reached with a transformer neutral point current of 60 A and a duration of 1,000 min or with a neutral point current of 10 A and a duration of 6000 min (100 h, 4.17 days). With this background, no transformer overheating is expected during the two presented GIC events during the five year observation period,considering the same transformer design as in Raith (2019). But we expect that increased moderate geomagnetic activity could cause a rise in transformer temperature. If an active transformer cooling system is installed and not already in full operation, the cooling system could be used to reduce the transformer operating temperature.

Besides uncertainties in geological structure, missing grid data is the main reason for differences between measurement and simulation (see e. g. the model results for #08 in **Figure 7**). A comparison of the magnetic field variation over time with the three closest INTERMAGNET observatories shows a congruent pattern. Therefore, the data from the single observatory (WIC) can be used in combination with the plane-wave method for GIC studies in Austria. The Austrian power grid is a non-steady, varying infrastructure over the measurement period of several years. This makes simulations difficult, as the current status of connections, outages or shutdowns is not known for every day since 2016. The resistances of transformers and lines are well known, but the substation grounding resistances are not available for all substations in Austria, and through experimentation with the simulation output vs. measurements, these have been found to have a large effect on the modelled GICs (a change of 0.1 Ω lead to a maximum change of 32 % or 2 A in the specific transformer neutral). A dedicated measurement campaign would be needed to gather more accurate grounding resistance data and account for this error source. During the commission of substations the state-of-the-art is to measure the substation earthing impedance with frequencies close to 50 Hz. In order to improve the simulation, a substation earthing resistance measurement with DC (0 Hz) and/or with low-frequencies (below 50/60 Hz nominal power system frequency).

Additionally, although we have data on the Austrian power grid, changes in neighboring countries are often unknown but still have influence on our calculations.

5 Conclusion

To conclude, we have presented an analysis of five years of DC measurements conducted with seven measurement systems at multiple locations in the Austrian power grid. The maximum measured amplitude during the observation period was 13.83 A during the geomagnetic storm on 2021 May 12th with a minimum Dst value of -61 nT. In addition to geomagnetic events and recurrent geomagnetic activity, we have identified the DC-powered public transportation system as a contributor to the grounded transformer neutral point currents. Other sources such as power electronic devices from renewable energy resources are also under investigation. Location-dependent daily recurring noise patterns have been detected in two sets of measurements and shown in **Figure 4c), d)**, but the sources have not been identified yet.

Correlations between changes in the magnetic field and changing neutral point currents during high geomagnetic activity are shown in **Figure 9**. This reveals location-dependent GIC sensitivity to specific directions of geomagnetic field changes, which is

also shown by the GIC fit method in the last column ofIn order to confirm the consistency of the measurement data, the correlation between the magnetic field changes and the changing neutral point current was calculated. The results reveals location-dependent GIC sensitivity to specific directions of geomagnetic field changes, which is also shown by the GIC fit method in the last column of **Table 1**.

Regarding the effects of GICs on transformer the 1 h GIC_{sum} value is calculated for the two presented events, revealing no transformer temperature increase could be expected during the events. A winding temperature increase is very unlikely, due to the values stated in Raith (2019), but cannot be excluded. Nevertheless, an individual transformer thermal-fleet screening should be carried out to determine the GIC sensitivity among the transformer types in the fleet.

The long term measurements in the Austrian power grid have already led to improvements in the simulation accuracy for GICs in the Austrian power grid by initiating further studies (not yet published) in the field of substation grounding calculation and sensitivity to various grid data. In addition to geomagnetic sources, we also identified other sources of low frequency currents. This work supports transmission grid operators to maintain and improve the grid availability and security. In the future, power grid assets and transformers endangered by GICs can be identified and protected by mitigation actions. In addition, other systems that interact with the power grid can be identified through continuous monitoring, providing reliable data to the system operation and utility manufacturers.

Acknowledgments

We would like to extend our thanks to APG for giving us the opportunity to set up and continuously operate the transformer neutral current measurements.

Data availability statement: The data this study is based on, namely the DC measurements in transformers in Austria, can not be openly shared due to grid safety concerns, however the data may be shared in part for smaller studies, and any interested party should contact the corresponding author for details. The geomagnetic field variations from the Conrad Observatory (WIC) used to model the geoelectric field in Austria can be found under `https://intermagnet.org/` or by contacting the Observatory personnel. The LFC simulator used to model the GICs in the grid can be found at `https://github.com/P-Schachinger/LFC_simulator`. The Dst used in this paper was provided by the WDC for Geomagnetism, Kyoto (`http://wdc.kugi.kyoto-u.ac.jp/wdc/Sec3.html`). The Kp values used in this paper were provided by the GZF German Research Centra for Geosciences, Potsdam (`https://isdc.gfz-potsdam.de/kp-index/`).

PS and DA thank the TU Graz, APG and Siemens Energy for funding. RLB thanks the FFG and ZAMG for funding. Supported by TU Graz Open Access Publishing Fund.

References

Ádám, A., Prácser, E., & Wesztergom, V. (2012). Estimation of the electric resistivity distribution (EURHOM) in the european lithosphere in the frame of the eurisgic WP2 project. *Acta Geodaetica et Geophysica Hungarica*, *47*(4), 377–387. doi: 10.1556/AGeod.47.2012.4.1

Albert, D., Halbedl, T., Renner, H., Bailey, R. L., & Achleitner, G. (2019). Geomagnetically induced currents and space weather - A review of current and future research in Austria. In *2019 54th International Universities Power Engineering Conference (UPEC)* (pp. 1–6). [Piscataway, New Jersey]: IEEE. doi: 10.1109/UPEC.2019.8893515

Albert, D., Schachinger, P., Renner, H., Hamberger, P., Klammer, F., & Achleitner, G. (2020). Field experience of small quasi DC bias on power transformers A first classification of low-frequency current pattern and identification of

sources. In *Cigre Session 48*. Paris. doi: 10.1007/s00502-020-00846-1

Alves, M. V., Echer, E., & Gonzalez, W. D. (2006). Geoeffectiveness of corotating interaction regions as measured by Dst index. *Journal of Geophysical Research: Space Physics*, *111*(A7). doi: 10.1029/2005JA011379

Bailey, R. L., Halbedl, T., Schattauer, I., Achleitner, G., & Leonhardt, R. (2018). Validating GIC Models With Measurements in Austria: Evaluation of Accuracy and Sensitivity to Input Parameters. *Space Weather*, *16*(7), 887–902. doi: 10.1029/2018SW001842

Bailey, R. L., Halbedl, T., Schattauer, I., Römer, A., Achleitner, G., Beggan, C. D., ... Leonhardt, R. (2017). Modelling geomagnetically induced currents in midlatitude Central Europe using a thin-sheet approach. *Annales Geophysicae*, *35*(3), 751–761. doi: 10.5194/angeo-35-751-2017

Bailey, R. L., & Leonhardt, R. (2016). Automated detection of geomagnetic storms with heightened risk of GIC. *Earth, Planets and Space*, *68*(1), 716. doi: 10.1186/s40623-016-0477-2

Beltle, M., Schühle, M., & Tenbohlen, S. (2017). Galvanic coupling of Direct Currents in Transmission Grids and its Effects on Power Transformers. In Institute of High Voltage and Power Transmission (Ed.), *20th International Symposium on High Votlage engineering*. Buenos Aires, Argentina. Retrieved 11.11.2021, from `https://www.researchgate.net/publication/319703163_Galvanic_Coupling_of_Direct_Currents_in_Transmission_Grids_and_its_Effects_on_Power_Transformers`

Bolduc, L. (2002). GIC observations and studies in the Hydro-Québec power system. *Journal of Atmospheric and Solar-Terrestrial Physics*, *64*(16), 1793–1802. doi: 10.1016/S1364-6826(02)00128-1

Boteler, D. H., Pirjola, R., Blais, C., & Foss, A. (2014). Development of a GIC simulator. In *2014 IEEE PES general meeting* (pp. 1–5). Piscataway, NJ: IEEE. doi: 10.1109/PESGM.2014.6939778

Boteler, D. H., & Pirjola, R. J. (1998). Modelling geomagnetically induced currents produced by realistic and uniform electric fields. *IEEE Transactions on Power Delivery*, *13*(4), 1303–1308. doi: 10.1109/61.714500

Boteler, D. H., & Pirjola, R. J. (2017). Modeling geomagnetically induced currents. *Space Weather*, *15*(1), 258–276. doi: 10.1002/2016SW001499

Choi, K.-C., Park, M.-Y., Ryu, Y., Hong, Y., Yi, J.-H., Park, S.-W., & Kim, J.-H. (2015). Installation of Induced Current Measurement Systems in Substations and Analysis of GIC Data during Geomagnetic Storms. *Journal of Astronomy and Space Sciences*, *32*(4), 427–434. doi: 10.5140/JASS.2015.32.4.427

Forbes, K. F., & St. Cyr, O. C. (2010). An anatomy of space weather's electricity market impact: Case of the PJM power grid and the performance of its 500 kV transformers. *Space Weather*, *8*(9). doi: 10.1029/2009SW000498

Fritsch, F. N., & Carlson, R. E. (1980). Monotone Piecewise Cubic Interpolation. *SIAM Journal on Numerical Analysis*, *17*(2), 238–246. doi: 10.1137/0717021

Gaunt, C. T., Cilliers, P. J., Heyns, M. J., Lotz, S. I., Chisepo, H. K., Adebayo, A. V., ... Oyedokun, D. T. O. (2020). Calculations leading to voltage stability and transformer assessment in the presence of geomagnetically induced currents. In *Cigre Session 48* (Vol. C4). Paris. Retrieved 26.08.2020, from `https://sessionpapersdoc.cigre.org/`

Geoforschungszentrum Potsdam. (2020). *Geomagnetic Observatories*. Retrieved 27.2.2020, from `https://www.gfz-potsdam.de/en/section/geomagnetism/infrastructure/geomagnetic-observatories/`

Gertmar, L., Karlsson, P., & Samuelsson, O. (2005). On DC injection to AC grids from distributed generation. In *European Conference on Power Electronics and Applications, 2005* (pp. 10 pp–P.10). Piscataway, NJ: IEEE Service Center. doi: 10.1109/EPE.2005.219420

Gil, A., Modzelewska, R., Wawrzaszek, A., Piekart, B., & Milosz, T. (2021). So-

lar Rotation Multiples in Space-Weather Effects. *Solar Physics*, *296*(8), 1–13. Retrieved from https://link.springer.com/article/10.1007/s11207-021-01873-7 doi: 10.1007/s11207-021-01873-7

Girgis, R., & Ko, C.-D. (1992). Calculation techniques and results of effects of GIC currents as applied to large power transformers. *IEEE Transactions on Power Delivery*, *7*(2), 699–705. doi: 10.1109/61.127070

Halbedl, T. (2019). *Low Frequency Neutral Point Currents on Transformer in the Austrian power Transmission Network* (PhD Thesis). Graz University of Technology, Graz.

Halbedl, T., Renner, H., Bailey, R. L., Leonhardt, R., & Achleitner, G. (2016). Analysis of the impact of geomagnetic disturbances on the Austrian transmission grid. In *19th Power Systems Computation Conference* (pp. 1–5). Piscataway, NJ: IEEE. doi: 10.1109/PSCC.2016.7540833

Halbedl, T., Renner, H., Sakulin, M., & Achleitner, G. (2014). Measurement and analysis of neutral point currents in a 400-kV-network. In *2014 Electric Power Quality and Supply Reliability Conference (PQ)* (pp. 65–68). Piscataway, NJ: IEEE. doi: 10.1109/PQ.2014.6866785

Kelbert, A. (2020). The Role of Global/Regional Earth Conductivity Models in Natural Geomagnetic Hazard Mitigation. *Surveys in Geophysics*, *41*(1), 115–166. doi: 10.1007/s10712-019-09579-z

Kellerman, A. C., Mcgranaghan, R., Bortnik, J., Carter, B. A., Hughes, J., Arritt, R. F., ... Yue, J. (2021). Geomagnetically induced currents at middle latitudes: 1. quiet-time variability. *Space Weather*, *n/a*(n/a), e2021SW002729. (e2021SW002729 2021SW002729) doi: https://doi.org/10.1029/2021SW002729

Lehtinen, M., & Pirjola, R. J. (1985). Currents produced in earthed conductor networks by geomagnetically-induced electric fields. *Ann. Geophysicae*, *3*, 479–484.

Lowes, F. J. (2009). DC railways and the magnetic fields they produce—the geomagnetic context. *Earth, Planets and Space*, *61*(8), i–xv. doi: 10.1186/BF03352944

Molinski, T. S. (2002). Why utilities respect geomagnetically induced currents. *Journal of Atmospheric and Solar-Terrestrial Physics*, *64*(16), 1765–1778. doi: 10.1016/S1364-6826(02)00126-8

Oughton, E. J., Skelton, A., Horne, R. B., Thomson, A. W. P., & Gaunt, C. T. (2017). Quantifying the daily economic impact of extreme space weather due to failure in electricity transmission infrastructure. *Space Weather*, *15*(1), 65–83. doi: 10.1002/2016SW001491

Pfeiffer, M., Franck, C. M., & Schmutz, J. (2015). DC ion-currents in AC conductors in hybrid AC/DC transmission systems. In *AC and DC Power Transmission 2015.* doi: 10.1049/cp.2015.0022

Pirjola, R. (1982). *Electromagnetic induction in the earth by a plane wave or by fields of line currents harmonic in time and space* (Ph Thesis, Finnish Meteorological Institute, Helsinki). Retrieved from https://books.google.at/books?id=s33DwQEACAAJ

Pirjola, R. (1989). Geomagnetically induced currents in the Finnish 400 kV power transmission system. *Physics of the Earth and Planetary Interiors*, *53*(3-4), 214–220. doi: 10.1016/0031-9201(89)90005-8

Price, P. R. (2002). Geomagnetically induced current effects on transformers. *IEEE Transactions on Power Delivery*, *17*(4), 1002–1008. doi: 10.1109/TPWRD.2002.803710

Pulkkinen, A., Pirjola, R., & Viljanen, A. (2007). Determination of ground conductivity and system parameters for optimal modeling of geomagnetically induced current flow in technological systems. *Earth, Planets and Space*, *59*(9), 999–1006. Retrieved from https://earth-planets-space.springeropen.com/

articles/10.1186/BF03352040 doi: 10.1186/BF03352040

Raith, J. (2019). *Risk Assessment of Power Transformers under the Influence of Geomagnetically Induced Currents (GIC)* (Doctoral Thesis, TU Graz, Graz). Retrieved 14.09.2021, from https://diglib.tugraz.at/risk-assessment-of-power-transformers-under-the-influence-of-geomagnetically-induced-currents-gic-2019

Richardson, I. G., Cliver, E. W., & Cane, H. V. (2000). Sources of geomagnetic activity over the solar cycle: Relative importance of coronal mass ejections, high-speed streams, and slow solar wind. *Journal of Geophysical Research: Space Physics*, *105*(A8), 18203–18213. doi: 10.1029/1999JA000400

Rodger, C. J., Mac Manus, D. H., Dalzell, M., Thomson, A. W. P., Clarke, E., Petersen, T., ... Divett, T. (2017). Long-Term Geomagnetically Induced Current Observations From New Zealand: Peak Current Estimates for Extreme Geomagnetic Storms. *Space Weather*, *15*(11), 1447–1460. doi: 10.1002/2017SW001691

Schachinger, P., & Albert, D. (2021). *LFC Simulator*. Institute of Electrical Power Systems. Retrieved 17.08.2021, from https://github.com/P-Schachinger/LFC_simulator

Simonyi, K. (1971). *Theoretische Elektrotechnik* (4., überarbeitete und ergänzte Auflage ed., Vol. Band 20). Berlin: VEB Deutscher Verlag der Wissenschaften.

Simpson, F. (2005). *Practical magnetotellurics*. Cambridge, UK and New York: Cambridge University Press. doi: 10.1017/CBO9780511614095

Torta, J. M., Serrano, L., Regué, J. R., Sánchez, A. M., & Roldán, E. (2012). Geomagnetically induced currents in a power grid of northeastern Spain. *Space Weather*, *10*(6), n/a-n/a. doi: 10.1029/2012SW000793

Tsurutani, B. T., Gonzalez, W. D., Gonzalez, A. L. C., Guarnieri, F. L., Gopalswamy, N., Grande, M., ... Vasyliunas, V. (2006). Corotating solar wind streams and recurrent geomagnetic activity: A review. *Journal of Geophysical Research: Space Physics*, *111*(A7). doi: 10.1029/2005JA011273

Zhang, J. J., Wang, C., Sun, T. R., Liu, C. M., & Wang, K. R. (2015). GIC due to storm sudden commencement in low-latitude high-voltage power network in China: Observation and simulation. *Space Weather*, *13*(10), 643–655. doi: 10.1002/2015SW001263